

Anisotropy of the Milky Way’s stellar halo using K giants from LAMOST and *Gaia*

SARAH A. BIRD,^{1,2} XIANG-XIANG XUE^{2,3}, CHAO LIU^{2,3}, JUNTAI SHEN^{1,3}, CHRIS FLYNN,⁴ AND
CHENGQUN YANG^{2,5}

¹*Shanghai Astronomical Observatory, 80 Nandan Road, Shanghai 200030, China*

²*Key Laboratory of Optical Astronomy, National Astronomical Observatories, Chinese Academy of Sciences, Beijing 100012, China*

³*College of Astronomy and Space Sciences, University of Chinese Academy of Sciences, 19A Yuquan Road, Beijing 100049, China*

⁴*Centre for Astrophysics and Supercomputing, Swinburne University of Technology, Post Office Box 218, Hawthorn, VIC 3122, Australia.*

⁵*School of Astronomy and Space Science, University of Chinese Academy of Sciences, Beijing 100049, China*

(Received July 2018; Revised; Accepted)

ABSTRACT

The anisotropy parameter β characterizes the extent to which orbits in stellar systems are predominantly radial or tangential, and is likely to constrain, for the stellar halo of the Milky Way, scenarios for its formation and evolution. We have measured β as a function of Galactocentric radius from 5 – 100 kpc for 7664 metal poor ($[\text{Fe}/\text{H}] < -1.3$) halo K giants from the LAMOST catalog with line-of-sight velocities and distances, matched to proper motions from the second *Gaia* data release. We construct full 6-D positions and velocities for the K giants to directly measure the three components of the velocity dispersion ($\sigma_r, \sigma_\theta, \sigma_\phi$) (in spherical coordinates). We find that the orbits in the halo are radial over our full Galactocentric distance range reaching over 100 kpc. The anisotropy remains remarkably unchanged with Galactocentric radius from approximately 5 to 25 kpc, with an amplitude that depends on the metallicity of the stars, dropping from $\beta \approx 0.9$ for $-1.8 \leq [\text{Fe}/\text{H}] < -1.3$ (for the bulk of the stars) to $\beta \approx 0.6$ for the lowest metallicities ($[\text{Fe}/\text{H}] < -1.8$). Considering our sample as a whole, $\beta \approx 0.8$ and, beyond 25 kpc, the orbits gradually become less radial and anisotropy decreases to $\beta < 0.3$ past 100 kpc. Within 8 kpc, $\beta < 0.8$. The measurement of anisotropy is affected by substructure and streams, particularly beyond a Galactocentric distance of approximately 25 kpc, where the Sagittarius stream is prominent in the data. These results are complimentary to recent analysis of simulations by Loebman et al. and of SDSS/*Gaia* DR1 data by Belokurov et al.

Keywords: galaxies: individual (Milky Way) — Galaxy: halo — Galaxy: kinematics and dynamics — Galaxy: stellar content — stars: individual (K giants) — stars: kinematics and dynamics

1. INTRODUCTION

The Milky Way’s halo has long provided constraints on scenarios for the formation and evolution of our galaxy, as it contains relics from the earliest stages of the process. In the dominant theoretical framework of galaxy formation, in which small scale structures condense most quickly under gravity in Λ CDM, Milky Way-like halos form early out of large numbers of minor and some major mergers, and have progressed well around the present day sized-Galaxy before the bulge and disk formation begins.

A fundamental constraint is provided by the stellar orbital families that develop during the assembly. The velocity anisotropy parameter β (Binney 1980; Binney & Tremaine 2008) characterizes the extent to which orbits in halos are predominantly radial or tangential and is defined through the velocity dispersions σ of the stars. Throughout this paper we use spherical coordinates (r, θ, ϕ) as described in Binney & Tremaine (2008, Appendix B)¹. In this system, the anisotropy parameter is defined as

$$\beta = 1 - (\sigma_\theta^2 + \sigma_\phi^2)/(2\sigma_r^2), \quad (1)$$

where $r = r_{\text{gc}}$ is the distance from the Galactic Center, θ is the polar angle $0 < \theta < \pi$ starting from the positive Z axis and increasing towards the $X - Y$ plane, and ϕ is the azimuthal angle $-2\pi < \phi < 2\pi$ for which $\phi = 0$ on the positive X axis and ϕ increasing towards the positive Y axis. In an isothermal system, $\sigma_\theta = \sigma_\phi = \sigma_r$, and $\beta = 0$. For stellar systems in which the

¹ Different coordinate systems (e.g. Cartesian, cylindrical, spherical), symbols (e.g. θ, ϕ), and schemes (e.g. (radial, polar, azimuthal), (radial, azimuthal, polar)) are used throughout the literature, which can be a source of possible confusion.

orbits are predominantly radial, $\beta > 0$. For predominantly tangential orbits, $\beta < 0$. By definition, $1 > \beta > -\infty$.

Hattori et al. (2017) and Loebman et al. (2018) have thoroughly reviewed the history of β measurement using halo stars within a few kpc of the Sun, programs to measure β from line-of-sight velocities out to tens of kpc from the Sun, and of the behavior of β in N -body and hydrodynamical simulations of Milky Way-like galaxies.

Until the advent of *Gaia*, large stellar samples with direct measurements of all three components of σ were limited to within the neighborhood of the Sun, i.e. within a few kpc. Locally, studies with e.g. RR Lyrae, K-giant, blue horizontal branch (BHB), and subdwarf stars find $\beta \approx 0.5$ -0.7, and the orbits are thus predominantly radial. For example², Morrison et al. (1990) derive $(\sigma_r, \sigma_\phi, \sigma_\theta) = (133 \pm 8, 98 \pm 13, 94 \pm 6)$ km s⁻¹ for halo G and K giants up to a few kpc distant ($(\sigma_r, \sigma_\theta, \sigma_\phi) = (133 \pm 8, 94 \pm 6, 98 \pm 13)$ km s⁻¹ for which $\beta \approx 0.5$). Chiba & Yoshii (1998) estimate $\beta = 0.52 \pm 0.07$ for a sample of halo stars ($[\text{Fe}/\text{H}] < -1.6$) within a few kpc of the Sun, based on the measurement of $(\sigma_U, \sigma_V, \sigma_W) = (161 \pm 10, 115 \pm 7, 108 \pm 7)$ km s⁻¹ ($(\sigma_r, \sigma_\theta, \sigma_\phi) \approx (161 \pm 10, 108 \pm 7, 115 \pm 7)$ km s⁻¹). Smith et al. (2009) find $\beta = 0.69 \pm 0.01$ using ≈ 1700 halo subdwarfs in SDSS Stripe 82 data up to 5 kpc distant, for which $(\sigma_r, \sigma_\phi, \sigma_\theta) = (143 \pm 2, 82 \pm 2, 77 \pm 2)$ km s⁻¹ ($(\sigma_r, \sigma_\theta, \sigma_\phi) = (143 \pm 2, 77 \pm 2, 82 \pm 2)$ km s⁻¹).

Efforts to understand whether such radial orbits are the case elsewhere in the Galaxy —

² We quote the results directly from the paper and in parentheses we rewrite the results into the spherical (r, θ, ϕ) system used in the current paper.

and particularly outside the Solar Circle — have been hampered by the lack of proper motions. The difficulties in accurately estimating velocity dispersions and velocity anisotropy, due largely to distance errors and lack of proper motions, are explored by, e.g., Schönrich et al. (2011); Beers et al. (2012); Fermani & Schönrich (2013), and Hattori et al. (2017). Out to a few tens of kpc, aided by models of the mass distribution in the Galaxy, line-of-sight velocities have been used to indirectly determine β from a range of tracers, including BHB stars, K giants, and F-type stars (Sommer-Larsen et al. 1994; Thom et al. 2005; Kafle et al. 2012, 2014; King et al. 2015, e.g.). Anisotropy has been measured using *HST* proper motion measurements for 13 main sequence turn-off halo stars with distance greater than ten kpc by Deason et al. (2013). Cunningham et al. (2016), as part of the HALO7D project, combine *HST* proper motions with line-of-sight velocities for 13 main sequence turn-off stars to measure β beyond ten kpc. As discussed in detail by Loebman et al. (2018), these studies have differed substantially in their results, with no clear picture of the behavior of β with Galactocentric radius emerging.

In this study, we use 7664 halo K giants for which we have radial velocities and stellar physical parameters (Wu et al. 2011; Luo et al. 2012; Wu et al. 2014) in the LAMOST data release DR5 (for information on LAMOST and its spectroscopic survey, we refer the reader to Cui et al. (2012), Deng et al. (2012), Zhao et al. (2012), and Luo et al. (2015)). Proper motions for the vast majority of these stars are available in the second data release (DR2) by *Gaia* (Gaia Collaboration et al. 2018) of April 2018. We compute V_r, V_θ, V_ϕ velocities of the halo giants as functions of Galactocentric radius r_{gc} and metallicity [Fe/H]. Substructure within the overall halo is clearly seen in the velocity-distance planes, such as the prominent Sagittarius stream (Belokurov et al. 2006). The velocity

dispersions of the radial and tangential components of the halo are found to differ substantially, and we present the anisotropy parameter β as a function of Galactocentric radius and stellar metallicity from this sample, finding that β is similar elsewhere in the halo as in the Solar neighborhood, with orbits very predominantly radial. We find nearly no dependence in β with Galactocentric radius r_{gc} out to approximately 25 kpc, despite the velocity dispersions changing markedly with r_{gc} . We additionally find that the amplitude of $\beta(r)$ reduces with decreasing metallicity, as has been found very recently for much more nearby main sequence halo stars by Belokurov et al. (2018). We compare our results for β to theoretical work using simulations of halo formation: these studies had successfully anticipated the result that the halo is predominantly radial, but to the best of our knowledge had not anticipated that β would show such metallicity dependence.

In Section 2, we present our sample of 7664 halo K giants, extending to over 100 kpc, for which we have LAMOST velocities, distances and metallicities, matched to *Gaia* DR2 proper motion data. In Section 3 we present the kinematics of the sample, and show that the orbital families are predominantly radial at all radii probed, through the anisotropy parameter β . We find that the amplitude of β is a function of metallicity, substantially reduced relative to the metal rich halo stars, but still radial. We discuss our results in terms of observational work in the literature, and N -body/hydrodynamical simulations of the formation and evolution of galaxy halos. In Section 4, we draw our conclusions.

2. LAMOST SAMPLE OF HALO K GIANTS

LAMOST has completed its fifth year of observing and has planned the data release of the LAMOST DR5 catalog for late 2018, to which we have acquired early access. Our halo K-giant sample has been selected using effec-

tive temperatures and surface gravities computed on the basis of spectral line features [Liu et al. \(2014\)](#). The specific selection criteria are $4000 < T_{\text{eff}}/\text{K} < 4600$ with $\log g < 3.5$ dex and $4600 < T_{\text{eff}}/\text{K} < 5600$ with $\log g < 4$ dex. As shown in [Liu et al. \(2014\)](#), these criteria select red-giant-branch stars over their full range of metallicities, and the contamination by stars other than K giants is small, $< 2.5\%$.

The distances for the halo K giants are estimated using the method of [Xue et al. \(2014\)](#), which we note is the same as the one used for Sloan Digital Sky Survey (SDSS) DR9 ([Ahn et al. 2012](#)) K-giant stars in the SEGUE project ([Yanny et al. 2009](#)). The photometry used in the distance estimation is from Pan-STARRS1 ([Chambers et al. 2016](#)) and SDSS and we calibrated Pan-STARRS1 to the SDSS photometric system. We use the reddening/extinction/dust maps of [Schlegel et al. \(1998\)](#) to estimate the extinction towards our stars. Studies show that these maps have biases which need to be corrected (e.g. [Cambrésy et al. 2005](#)). Our sample stars are all more than 5 kpc above the Galactic disk, so the extinctions derived from the [Schlegel et al. \(1998\)](#) maps, which are dominated by dust closer than 1 kpc to the Galactic plane, are appropriate. We assume the extinction at infinity for our halo star sample. Alternative maps are also available to be used, for example [Hakkila et al. \(1997\)](#), [Cambrésy et al. \(2005\)](#), and [Schlafly & Finkbeiner \(2011\)](#). We convert the [Schlegel et al. \(1998\)](#) $E(B - V)$ to SDSS filters using the conversion coefficients found on Table 6 of [Schlafly et al. \(2012\)](#) (for $R_V = A(V)/E(B - V) = 3.1$, the traditional value for the diffuse interstellar medium ([Cardelli et al. 1989](#))). We use the same luminosity ($\propto L^{-1.8}$) and density ($\propto r^{-3}$) profile priors for the [Xue et al. \(2014\)](#) Bayesian method, and the LAMOST K-giant $[\text{Fe}/\text{H}]$ distribution as the metallicity prior. The Bayesian method allows the uncertainties of the input values,

namely apparent magnitude, color, and metallicity, to be propagated properly to the final derived distances. More detailed analysis is described in [Xue et al. \(2014\)](#) for data from SDSS and similar conclusions can also be made for our LAMOST sample of halo K giants. The propagated uncertainties for SDSS K giants yield a median distance precision of 16% and for LAMOST K giants of 13% (see Fig. 1). The smaller median relative distance uncertainty for LAMOST K giants is due to smaller errors in Pan-STARRS1 photometry and LAMOST metallicities compared to the SDSS photometry and metallicities used for SDSS K giant distances. We note that the difference is small and thus the distances and uncertainties are comparable for LAMOST and SDSS K giants. Using the method presented in [Xue et al. \(2014\)](#), we select giant branch stars from above the horizontal branch to the tip of the red-giant branch. [Xue et al. \(2014\)](#) derived a relation between $[\text{Fe}/\text{H}]$ and the $(g - r)_0$ color of the giant branch at the level of the horizontal giant branch, using eight globular clusters with *ugriz* photometry from [An et al. \(2008\)](#), with cluster data given in Table 3 of [Xue et al. \(2014\)](#). The $[\text{Fe}/\text{H}]$ and $(g - r)_0^{\text{HB}}$ for the horizontal branch/red clump of the clusters follow a quadratic polynomial, $(g - r)_0^{\text{HB}} = 0.087[\text{Fe}/\text{H}]^2 + 0.39[\text{Fe}/\text{H}] + 0.96$, as shown in Fig. 2 of [Xue et al. \(2014\)](#). We work with giants above the horizontal branch to avoid possible contamination by (metal rich) red clump stars, and also in order to probe as distantly as possible in the halo by using the brightest giants.

We have compared the [Xue et al. \(2014\)](#) distances to distances derived by [Bailer-Jones et al. \(2018\)](#) using *Gaia* DR2 parallaxes. We select K giants within 4 kpc of the Sun where distances derived by parallax are accurate, and stars with $[\text{Fe}/\text{H}] < -1.0$ dex. In order to increase our sample size when estimating distances with the [Xue et al. \(2014\)](#) method, we use photometry

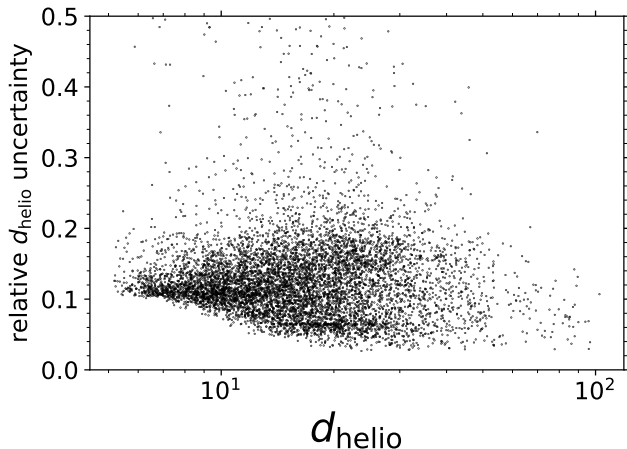


Figure 1. Relative distance uncertainties for our halo K-giant sample, shown as a function of heliocentric distance d_{helio} .

from Pan-STARRS1, SDSS, and additionally APASS (AAVSO Photometric All-Sky Survey, Henden & Munari 2014; Henden et al. 2015, 2016), as this boosts the sample size. We finally select only stars with relative distance uncertainty better than 40% ($\Delta d_{\text{helio}}/d_{\text{helio}} < 0.4$) for both methods. Fig. 2 shows the results. The top panels show histograms of the ratio of the two distance scales (denoted d_{CBJ} and d_{Xue} for Bailer-Jones et al. (2018) and Xue et al. (2014), respectively). There is close agreement between the scales, although we find there is an approximately 10% difference between the distance scales, with the Bailer-Jones et al. (2018) being greater on average (lower panels). This has small systematic effect on the anisotropy measurements of the halo sample, and is discussed further in Section 3.3. Adopting the Bailer-Jones et al. (2018) scale instead of the Xue et al. (2014) scale reduces the anisotropy parameter β somewhat (see Section 3.3 and Fig. 7).

Besides selecting K giants from LAMOST, Liu et al. (2014) also provide a distance calculation method for K giants. Liu et al. (2014) used 2MASS (Cutri et al. 2003; Skrutskie et al. 2006) photometry and synthetic isochrones to derive distances, also using a Bayesian method sim-

ilar to Xue et al. (2014). We choose to use the method of Xue et al. (2014) for several reasons. Photometry from Pan-STARRS1 and SDSS, which is used by the method of Xue et al. (2014), is more suitable for our K-giant sample than 2MASS. Xue et al. (2014) use globular cluster fiducials observed by SDSS. Due to these reasons, the Xue et al. (2014) method is more precise and we choose to use these distances.

Our sample consists of stars with $[\text{Fe}/\text{H}] < -1.3$ and which are well above and below the Galactic disk, using the cut $|Z| > 5$ kpc (where Z is height above the Galactic disk mid-plane).

The heliocentric line-of-sight LAMOST velocities need to be corrected by adding 5.7 km s^{-1} , a systematic bias which has been calculated by comparing LAMOST velocities to SDSS/SEGUE (Tian et al. 2015) and to *Gaia* (Schönrich & Aumer 2017). The LAMOST giants were cross-matched to *Gaia* DR2 to attain proper motions. Our total sample consists of 7664 halo K giants with distances, line-of-sight velocities, and proper motions.

We derive Galactocentric Cartesian coordinates (X, Y, Z) and velocities (U, V, W) using the conventions in *astropy* (Astropy Collaboration et al. 2018). The Sun is located at $X_{\odot} = -8.3$ kpc and $Z_{\odot} = 29$ pc. The local standard of rest (LSR) velocity is $v_{\text{lsr}} = 220$ km s^{-1} , and the motion of the Sun with respect to the LSR is $(U, V, W)_{\odot} = (11.1, 12.2, 7.3)$ km s^{-1} (Schönrich et al. 2010). We have tested different values for X_{\odot} (8 kpc), V_{lsr} (190, 250 km s^{-1}), V_{\odot} (1, 25 km s^{-1} , which are extreme values taken from Robin et al. (2017) and Bovy (2015), respectively), and W_{\odot} (20 km s^{-1}) and conclude that our main results remain unchanged.

We define spherical coordinates (r, θ, ϕ) and the corresponding spherical velocity components $(V_r, V_{\theta}, V_{\phi})$ using the following conven-

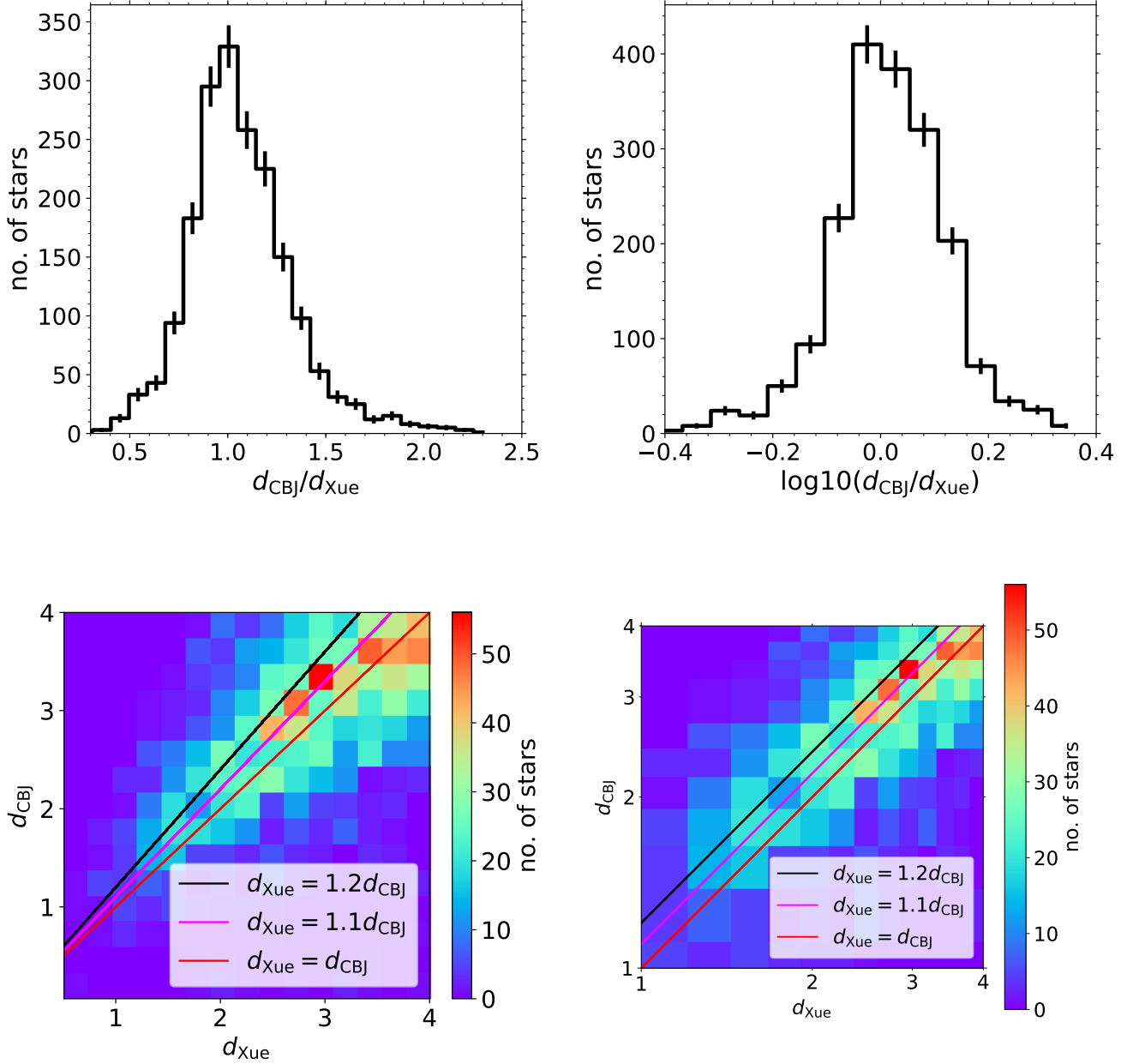


Figure 2. Comparison of the heliocentric distances d_{CBJ} estimated by Bailer-Jones et al. (2018) to the heliocentric distances d_{Xue} of Xue et al. (2014), for halo K giants ($[\text{Fe}/\text{H}] < -1$) in LAMOST data and within 4 kpc of the Sun. **Upper panels:** histograms of the ratio $d_{\text{CBJ}}/d_{\text{Xue}}$ shown in linear and log scales. The histograms show a systematic difference between the two distance scales of 10%, in the sense that the Xue et al. (2014) distances are closer by 10% on average than those of Bailer-Jones et al. (2018). **Lower panels:** density map comparisons of the distances estimated by Bailer-Jones et al. (2018) to those of Xue et al. (2014). Note the axes are linear in the left panel and logarithmic in the right panel. The lines mark the 1:1 relation between the scales, and systematic shifts of 10% and 20% between them.

tion³:

$$r_{\text{gc}} = \sqrt{X^2 + Y^2 + Z^2} \quad (2)$$

$$\theta = \pi/2 - \tan^{-1}(Z/\sqrt{X^2 + Y^2}) \quad (3)$$

$$\phi = \tan^{-1}(Y/X) \quad (4)$$

$$V_r = (U \cos \phi + V \sin \phi) \sin \theta + W \cos \theta \quad (5)$$

$$V_\theta = (U \cos \phi + V \sin \phi) \cos \theta - W \sin \theta \quad (6)$$

$$V_\phi = U \sin \phi - V \cos \phi. \quad (7)$$

Gaia parallaxes are available for a subset of the stars, but only become competitive with the LAMOST distances for stars closer than approximately 4 kpc. We therefore use LAMOST distances for all our stars, as the cut $|Z| > 5$ kpc (to remove disk and/or thick disk stars) means matches to *Gaia* have larger relative errors in *Gaia* parallaxes as compared to our relative photometrically determined distance errors.

3. RESULTS

3.1. Sample kinematics and the halo anisotropy

In Fig. 3, we show the 3-D velocities V_r, V_θ, V_ϕ for our halo sample as functions of metallicity $[\text{Fe}/\text{H}]$ (left panels) and Galactocentric radius r_{gc} (right panels). We have very conservatively cut the sample to metallicities $[\text{Fe}/\text{H}] < -1.3$, based on our estimated metallicity errors of 0.1 dex, in order to probe the halo only (examination of a fuller data set of LAMOST K giants, for metallicities up to Solar ($[\text{Fe}/\text{H}] = 0$), shows that the disk-to-halo transition occurs at $[\text{Fe}/\text{H}] = -1$ for the stars analyzed (for which $|Z| > 5$ kpc)). The K-giant velocities are clearly those of a nearly non-rotating, pressure supported population, with no sign of a much

faster rotating thick disk (or disk) at our highest metallicities ($[\text{Fe}/\text{H}] = -1.3$). In the right-hand panels, we show the velocities as a function of Galactocentric distance r_{gc} . Although the bulk of the stars are within 30 kpc of the Galactic Center, we have sufficient numbers of stars to probe β out to 100 kpc. There is very clearly substructure on different scales in the velocity distributions versus Galactocentric distance. The most obvious substructure is due to the Sagittarius stream (e.g. [Ibata et al. 1994](#); [Majewski et al. 2003](#); [Belokurov et al. 2006](#)), seen in (V_r, V_θ) at $V_r \approx -180, -80 \text{ km s}^{-1}$ and $V_\theta \approx 200 \text{ km s}^{-1}$. In Section 3.2 and Fig. 6, we introduce a simple selection in energy E and total angular momentum L space which we use to remove the strongest overdense region visible by eye in E - L space. These stars we associate as likely Sagittarius members and mark them as small red crosses in Fig. 3.

[Carlin et al. \(2016\)](#) have analyzed the extent to which substructures can be isolated in K giants in LAMOST, by comparing to ensembles of smooth, synthetic Milky Way models finding that at least 10% of the stars can be associated with streams and other debris. Structures become prominent beyond a Galactocentric radius of approximately 20 kpc within an otherwise well-mixed halo, while beyond approximately 40 kpc, star numbers in the catalog are insufficient to draw conclusions on the sub-structure fraction. The strongest substructure they find is due to the Sagittarius stream.

We next compare velocity dispersions and β for the total data set, with and without Sagittarius stars included. The aim is to examine the extent to which the most prominent of substructures, Sagittarius, affects the determination of β . Structures seen in space and velocity coordinates are considered likely “un-relaxed” and “non-virial” components within the Galactic halo. As has been shown in detail in [Loebman et al. \(2018\)](#), the anisotropy parameter is

³ Note: the $\tan^{-1}(y/x)$ functions have been implemented in our Python code using the 2-argument arctangent function `numpy.arctan2(y,x)`, which takes into account the signs of x and y .

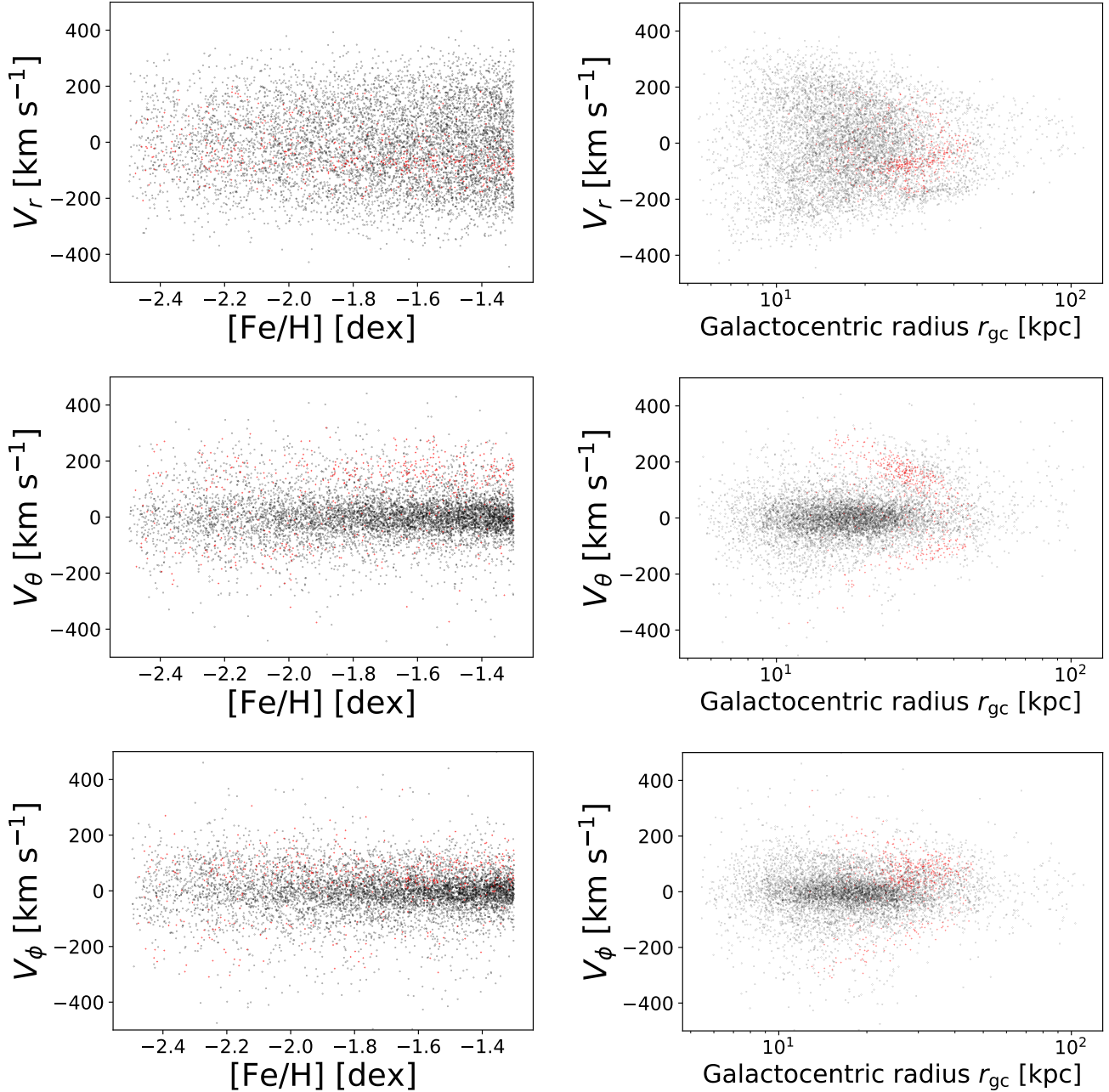


Figure 3. The space velocities in spherical coordinates (r, θ, ϕ) are shown for our sample of 7664 halo K giants (black dots and small red crosses) for which we have LAMOST line-of-sight velocities and metallicities, and *Gaia* proper motions. In the left panels, the velocities are shown versus metallicity $[\text{Fe}/\text{H}]$, and in the right panels versus Galactocentric distance r_{gc} . We use the energy versus total angular momentum E - L plane to flag an overdense region of stars as those predominantly belonging to Sagittarius (see Section 3.2 and Fig. 6). We propagate our E - L selected Sagittarius-member stars in red in the left and right panels to view their characteristics in Galactocentric distance, velocity, and metallicity. In the right panels in particular, several substructures in the kinematics are clear, including that due to the Sagittarius stream discussed in Section 3.2. The Galactocentric radial velocities V_r show a considerably broader distribution than either of the tangential velocity components V_θ and V_ϕ : the orbital families are predominantly radial. This becomes distinctly less the case for the lowest metallicities probed (left panels, $[\text{Fe}/\text{H}] < -2$), as discussed in Section 3.4, although the orbits are still predominantly radial.

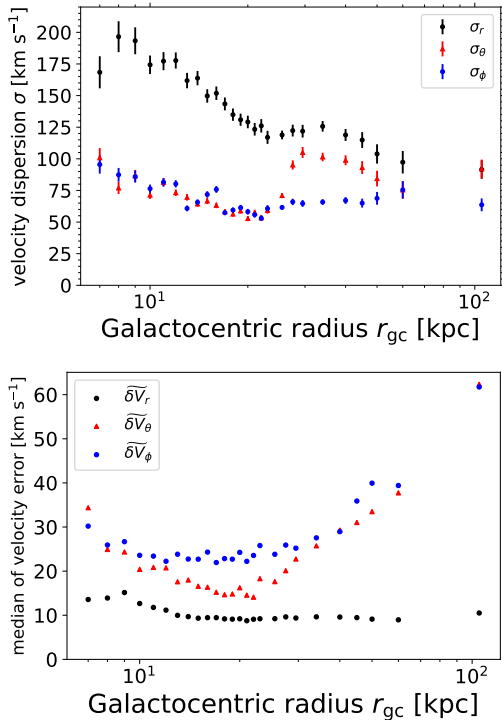


Figure 4. Upper panel: three velocity dispersion components ($\sigma_r, \sigma_\theta, \sigma_\phi$) computed from the total sample of 7664 halo K giants. Each marker represents the end of our selected radial bins. The first bin contains stars within $r_{gc} = 5-7$ kpc. Each consecutive bin is of width 1 kpc up to the bin ending at $r_{gc} = 30$ kpc, after which our bin sizes progressively increase. The remaining bins end at $r_{gc} = 32, 35, 40, 45, 50, 60,$ and 105 kpc. Error bars are estimated from the Poissonian sampling in each bin. **Lower panel:** median errors ($\delta V_r, \delta V_\theta, \delta V_\phi$) on the velocities as a function of Galactocentric radius, for the same bins as in the upper panel. The error estimates for each star are propagated from the LAMOST distance errors, LAMOST line-of-sight velocity errors, and two proper motion error estimates from *Gaia* DR2.

sensitive to both the presence of satellites in the halo, and to the passage of satellites through the underlying, smooth and kinematically relaxed stellar halo.

In the upper panel of Fig. 4, we show the velocity dispersions ($\sigma_r, \sigma_\theta, \sigma_\phi$) as functions of Galactocentric radius r_{gc} . These have been estimated from the component velocities using

ROBUST_SIGMA⁴, which is designed particularly to reduce the effects of outliers in otherwise relatively Gaussian distributions. We have subtracted in quadrature the median of the velocity errors ($\delta V_r, \delta V_\theta, \delta V_\phi$) of the stars in each bin. These errors are as propagated from the (1) errors in the LAMOST distances of the stars (16%), (2) the LAMOST line-of-sight radial velocity errors (generally in the range 5 to 25 km s⁻¹), (3) and the two proper motion error estimates from *Gaia* DR2. For most bins the corrections are quite small, but do grow with Galactocentric distance as the stars become fainter, and the proper motions smaller, as seen in the lower panel of Fig. 4. In the most distant bins the corrections are about the same magnitude as the velocity dispersion we are aiming to measure. For less than 1% of the stars, velocities in excess of 500 km s⁻¹ were obtained. These are very likely to be spurious rather than true high velocity stars, and were removed from the final sample (such high velocities are clipped by ROBUST_SIGMA in the analysis in any case). Additionally, for approximately 1% of the stars, spuriously high errors were found for the V_r, V_θ and/or V_ϕ velocities. Such stars were removed from the sample by requiring that the error on the Galactocentric radial velocity be < 100 km s⁻¹, and the error on the tangential velocities be < 150 km s⁻¹. Tests with or without these criteria showed that these cuts barely affect β , but we include them for completeness.

The upper panel of Fig. 4 shows σ_r and the two tangential velocity dispersions σ_θ and σ_ϕ as functions of Galactocentric radius for our complete sample of halo K giants. It is clear that both tangential dispersions are substantially less than the radial velocity dispersion σ_r

⁴ ROBUST_SIGMA (Freudenreich et al. 1990-2009) is a routine from IDL ASTROLIB (Landsman 1993). We use a port to Python.

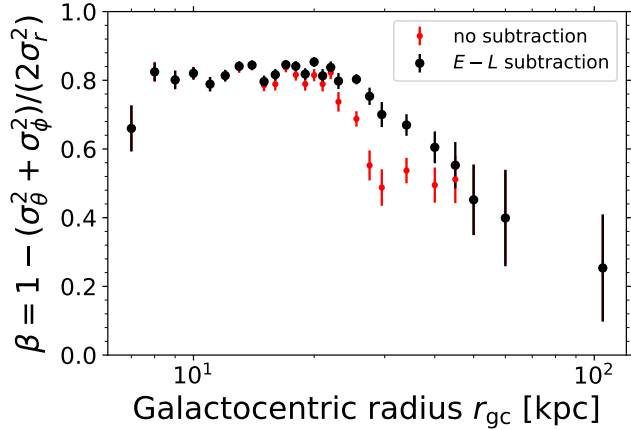


Figure 5. Anisotropy parameter β as a function of Galactocentric radius r_{gc} for the entire sample of 7664 halo K giants (red dots) and for the sample with Sagittarius flagged and removed (remaining sample of 7182 K giants, black dots), to highlight the effect of this substructure in the sample. The error bars on β are propagated through from the errors in measuring σ_r , σ_θ and σ_ϕ (cf. Fig. 4, upper panel). We see a dip from 25 to 40 kpc of the red-dot β profile, due to the effects of the Sagittarius stream (we select the stream stars in Fig. 6). Removing these stars takes a strongly tangential orbital family out from the sample, making β more radial by ~ 0.2 .

at all radii out to almost 100 kpc. The orbits are clearly strongly radial throughout the halo.

We highlight this in Fig. 5, where we show the orbital anisotropy parameter β versus Galactocentric radius r_{gc} for the entire sample (i.e. without Sagittarius stars removed, red dots). The halo orbits are strongly radial, with β lying mainly in the range 0.6 to 0.8. It is remarkable how steady β is with Galactocentric radius r_{gc} , out to about 25 kpc, despite the considerable change in the underlying σ_r and the two tangential velocity dispersions as functions of r_{gc} . Simulated stellar halos typically show a steady or very slowly rising β profile for $r_{gc} > 5$ kpc (see e.g. Diemand et al. (2005), Abadi et al. (2006), Rashkov et al. (2013)), which is consistent with what we see out to about 25 kpc in Fig. 5. Loebman et al. (2018) have analyzed

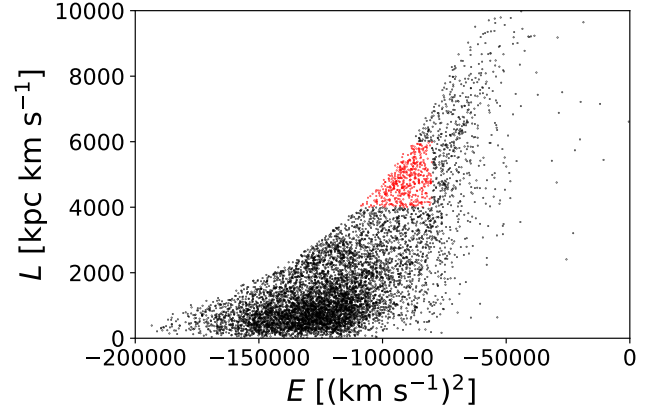


Figure 6. Energy E versus total angular momentum L for the full sample of 7664 halo K giants (black and red dots). Energies for the stars have been estimated using a Milky Way-like potential consisting of an NFW dark halo and a double exponential disk using `galpy` (Bovy 2015). We flag the overdense region of stars marked in red in this E - L plane as predominantly in the Sagittarius stream.

the simulated stellar halos of Bullock & Johnston (2005), Christensen et al. (2012), and Stinson et al. (2013), finding that (unless the galaxies are in a state in which major merging is still taking place) β remains high (in the range 0.6 to 0.8) out to the limits of their analysis (70 kpc). This is quite different to what we see in Fig. 5, where there is decline from $\beta \approx 0.8$ to $\beta \approx 0.2$ out to 100 kpc, at the limits of our sample. To the best of our knowledge, no such behavior has been seen in simulated stellar halos. It will be very interesting to examine to what extent this is inconsistent with the halo stars seen in stellar halo simulations at these large distances, work we leave for the future.

We have validated our analysis codes for determining β as a function of Galactocentric radius via mock data sets. The mocks are based on the halo K-giant sample as follows: we set up a range of models for $\beta(r_{gc})$ as a function of Galactocentric radius r_{gc} , and assign velocities V_r, V_θ, V_ϕ to each star in the sample based on its Galactocentric distance and the error estimates on V_r, V_θ, V_ϕ propagated through from

the LAMOST and *Gaia* error estimates (in distance, line-of-sight velocities, and proper motions). Having imposed a particular functional form for β on the data set stars, we test our ability to recover it using the methods applied to the actual data. We tested a range of models for β : isothermal ($\beta = 0$), strongly radially anisotropic ($\beta = 0.75$), strongly tangentially anisotropic ($\beta = -1$), and models for which β is a function of r_{gc} (e.g. Sommer-Larsen et al. 1994). We find that even with the quite large errors that develop in the tangential velocities at large distance (of order the velocity dispersion of the stars) seen in Fig. 4, we are able to recover β correctly. These tests confirm that the dominant source of uncertainty is Poisson statistics in the bins for our particular sample of halo giants. We note that we provide no extensive test of anisotropy models with narrow features, such as the sharp dips in β as a function of Galactocentric radius seen by Kafle et al. (2012). Such features would be poorly resolved in this study of halo K giants because of distance errors, as already pointed out by Hattori et al. (2017) and Loebman et al. (2018), and the existence of such features is difficult to test with the current data set.

3.2. Effects of substructure

Simulations of stellar halos in Milky Way type galaxies show that the anisotropy β with Galactocentric radius is sensitive to the presence of satellites and streams within the overall halo population, as might be expected, but also to the passage of satellites affecting the orbital parameters of the underlying, smooth, and kinematically relaxed stellar halo (Loebman et al. 2018).

We do not make detailed analysis of such effects in this paper, but restrict ourselves to a brief examination of Sagittarius (the most prominent substructure in the velocity plots). There are a number of ways in which its stars could be removed from the sample in order to

examine how they are currently affecting the β profile: we have chosen the simplest expedient of tagging Sagittarius in energy E versus total angular momentum L . We achieve this by equating Sagittarius with the most prominent overdensity in the E - L plane. We note that E versus the vertical angular momentum L_Z would be a better choice for isolating Sagittarius stars over e.g. many orbits in an axisymmetric potential as both these quantities are conserved (whereas L may only be approximately conserved), but that is not our aim here.

The full sample is shown in the E - L space in Fig. 6, where we have adopted, again for simplicity, a Milky Way-like potential $\Phi(R, Z)$ in the `galpy` package (Bovy 2015) composed of an NFW dark halo and a double exponential disk, to order the stars by an energy, E :

$$E = \Phi(R, Z) + V_{\text{tot}}^2/2, \quad (8)$$

where $R = \sqrt{X^2 + Y^2}$ and V is the total velocity of the star ($V_{\text{tot}}^2 = U^2 + V^2 + W^2 = V_r^2 + V_\theta^2 + V_\phi^2$). The total angular momentum L is

$$L = r_{\text{gc}} V_{\text{tan}}, \quad (9)$$

where V_{tan} is the total tangential velocity ($V_{\text{tan}}^2 = V_\theta^2 + V_\phi^2$).

To the eye, the E - L plane shows two major substructures in addition to the bulk of the halo stars seen at the bottom of the plot. Kinematic substructures appear prominently in E - L space, due to common energy and angular momentum. The most prominent overdensity in the E - L plane is found at $E = -90000$ (km s⁻¹)² and $L = 5000$ kpc km s⁻¹. We equate this overdensity as being predominantly composed of Sagittarius stars and select a region surrounding the overdensity (in E - L space) to cut from our sample as a simple method to test the effects on β due to Sagittarius. We define an arbitrary box in E - L space with appropriate size to enclose the overdensity we wish to remove. We define limits of the region in which

to remove the stars as $E < -80000$ (km s^{-1})² and $4000 < L < 6000$ kpc km s^{-1} (marked in red in Fig. 6) and recompute the $\beta(r)$ profile. The stars separate out well in this space because of Sagittarius’ high latitude, tangential orbit. We propagate our selection from the E - L plane to the Galactocentric distance, velocity, and metallicity planes shown in Fig. 3 (small red crosses). Our selected stars from the E - L space well-cover the most prominent features of Sagittarius seen in the r_{gc} - V_θ space and r_{gc} - V_r space ($(V_r, V_\theta) \approx (-180, 200)$ and $\approx (-80, 200)$ km s^{-1}). That stars which we select with our simple cut in E - L space also appear in the same region as Sagittarius in the Galactocentric distance and velocity spaces gives us confidence that we can use our simple E - L as an initial exploration of the effects of Sagittarius on β . After using the E - L criteria to remove the stars that we associate with Sagittarius, we show the resulting profile in Fig. 5 (black dots).

The $\beta(r)$ profile with Sagittarius still in the sample is shown by the red dots, and the profile with Sagittarius removed is shown by the black dots. In the region where Sagittarius contributes most strongly to the anisotropy profile, from 25 to about 40 kpc, β becomes more radial but only mildly so, rising by one to two tenths. This is in line with expectation, as Sagittarius is on a high latitude, tangential orbit, and biases β to appear more tangential (lower values of β). We note that outside the regions in Galactocentric radius where Sagittarius is having an impact, β is barely affected.

This brief look at the most prominent substructure in the sample shows that even a quite massive satellite passing through the underlying stellar halo can have modest effects on β in the sense that the overall stellar halo orbits remain very radial. It is interesting that the break in the β profile, from a remarkably steady value at $\beta \approx 0.8$ from the Sun to 20 kpc, occurs where Sagittarius starts to make its presence felt. This

behavior, in which β has breaks or dips as a function of r_{gc} , is similar to that seen in simulations of the formation and evolution of the halo component in N -body/hydrodynamical simulations analyzed in detail by Loebman et al. (2018). A simple view is that the break is from a quite well mixed inner halo within approximately 25 kpc, where the orbital families and β are in (currently) a steady state to regions where substructure is affecting β via satellite infall and streams. Clearly the effects of substructure are a major topic and we leave this to future work, but point out that even the most prominent substructure in our sample only affects β modestly. It is unlikely that the remaining, much weaker, substructures seen in the velocity plots will affect the conclusion that the halo K giants in our sample have strongly radial orbits.

3.3. Effects of distance bias

The adopted distance scale for our K giants was cross-checked in Section 2, where we compared our halo K-giant distance scale to that of Bailer-Jones et al. (2018), for halo K giants within approximately 4 kpc of the Sun. This test showed evidence for our distances being closer on average than the Bailer-Jones et al. (2018) distances by approximately 10% (Fig. 2). Bailer-Jones et al. (2018) use a model of a “lengthscale” at any given (l, b) position, to derive improved distance estimates of stars compared to simply inverting the parallax. The modeling is validated using stars in open clusters, i.e. on metal rich stars. The Xue et al. (2014) distances have been calibrated using K giants in globular clusters, stars very similar to our halo K giants. A systematic distance correction for our sample stars will have the effect of increasing the estimated tangential velocity dispersions (which are primarily sensitive to the distance scale via proper motions), while leaving the Galactocentric radial velocity dispersions relatively unaffected (as these are typically dominated by line-of-sight velocities).

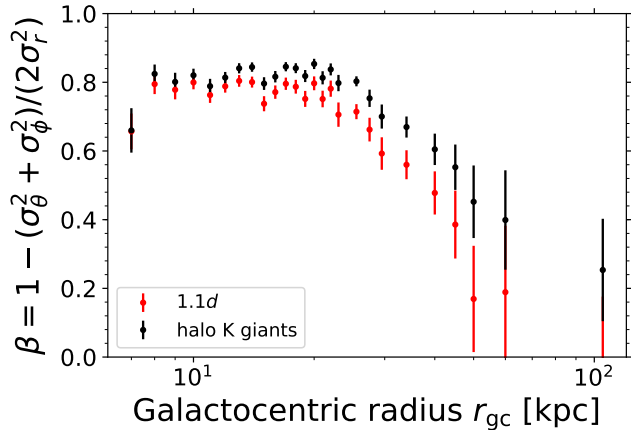


Figure 7. The effect on the estimates of the anisotropy parameter β if we adopt a systematic correction to our distance scale for halo K giants of 10%, to bring the giants into agreement with the distance scale for nearby halo K giants due to Bailer-Jones et al. (2018). Black symbols show β for the Xue et al. (2014) distance scale, and red symbols show β for this distance scale increased by 10%.

Consequently we expect such a distance correction to reduce the estimates of the anisotropy β slightly. We show this in Fig. 7 using our halo K-giant sample after removing Sagittarius. The anisotropy β decreases very slightly in the inner halo ($r_{gc} < 30$ kpc) as a result of this correction although it decreases somewhat more in the outer halo. This shows that the main result of the paper, that the bulk of the halo K giants are on highly radial orbits, is very robust to systematic error in the distance scale of this order.

3.4. Metallicity dependence of the anisotropy

We have examined the behavior of $\beta(r)$ as a function of the metallicity of the stars. After removing Sagittarius stream stars, selecting stars over the metallicity range $-2.5 < [\text{Fe}/\text{H}] < -1.3$, and dividing them into three roughly equally populated bins in this range, we have plotted $(\sigma_r, \sigma_\theta, \sigma_\phi)$ and β versus r_{gc} for each subset, as shown in Fig. 8. Interestingly, for the metal poor bin ($-2.5 < [\text{Fe}/\text{H}] < -1.8$), we

find a significantly lower β at 0.6, compared to 0.9 for the rest of the sample. Beyond 25 kpc, the two more metal rich bins steadily decline in anisotropy whereas the more metal poor bin remains relatively constant; but we note that substructure clearly affects β and any trends should be treated with caution.

A picture has emerged in recent years of a two-component halo which differs in spatial distributions of metallicity, age, and kinematics (e.g. Carollo et al. 2007; Deason et al. 2011). The same formation and evolution processes responsible for the dichotomy found in the stellar halo are also likely to affect the anisotropy of the orbits. Indeed, Hattori et al. (2013) and Kafle et al. (2013), in studies of halo BHB stars within a few tens of kpc, have noted that anisotropy is a function of metallicity. In both studies, the halo stars are subdivided into two metallicity bins at $[\text{Fe}/\text{H}] = -2$, and the difference in the kinematics (i.e. anisotropy and the bulk rotation) of the two sub-samples is argued to support the two-component picture for the halo. They find that the lower metallicity stars have rounder orbits — although the anisotropy obtained is significantly lower than what we find for our metal poor stars (we find $\beta \approx 0.6$ whereas they find much rounder orbits, with $\beta \approx 0$ to -1).

It is very instructive to compare our sample to Belokurov et al. (2018), who have analyzed the anisotropy properties of a sample of main sequence halo stars, for which, as here, full kinematical and metallicity data are available. Their sample have been selected from SDSS and *Gaia* DR1, and are within ≈ 10 kpc of the Sun. They find similar results for nearby stars to what we have found in the distant halo. The orbits of the bulk of the nearby halo stars are highly radial $\beta \approx 0.9$, with β declining to more mildly radial orbits ($0.2 < \beta < 0.4$) down to the lowest metallicities probed ($[\text{Fe}/\text{H}] \approx -3$). This decline in β with metallicity is similar to what

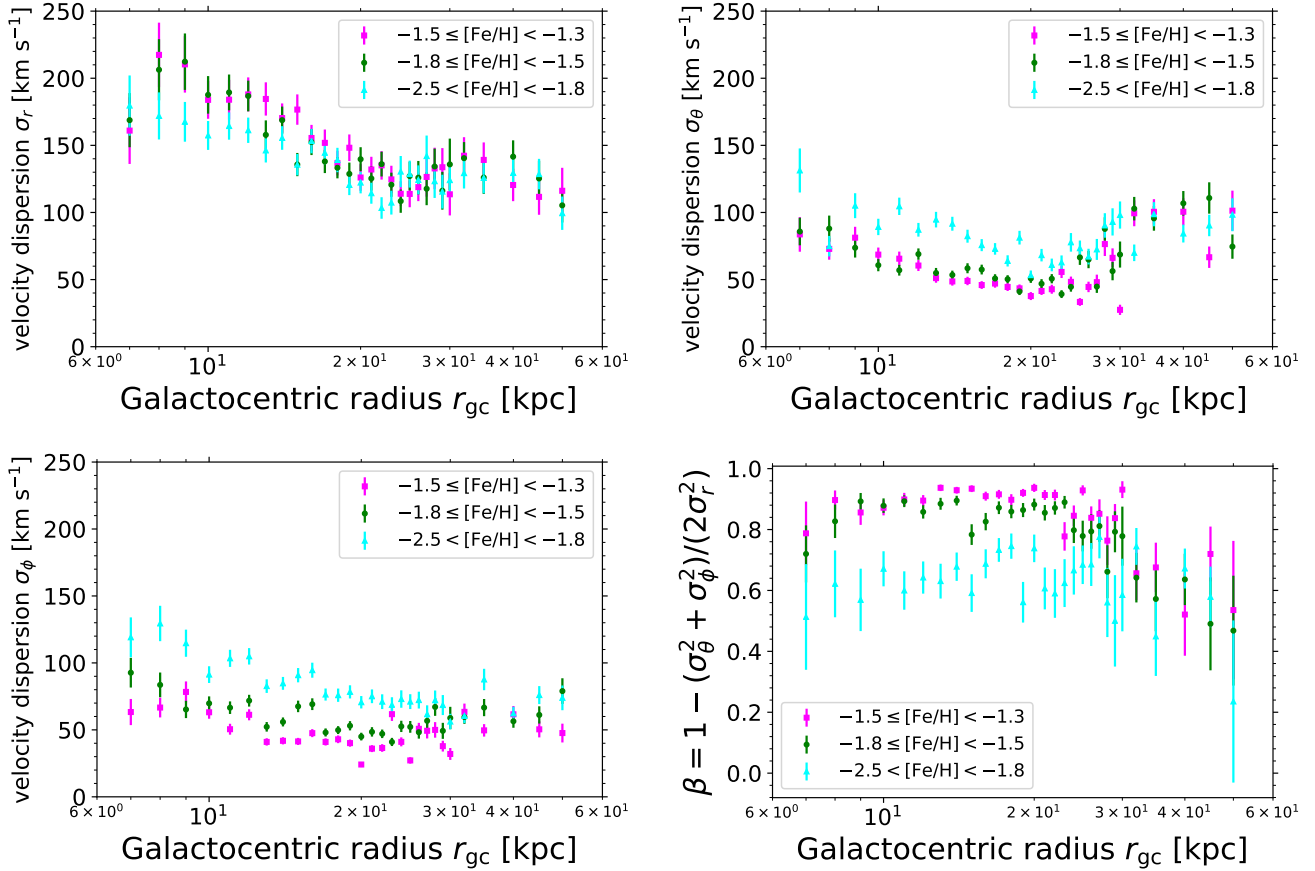


Figure 8. Profiles in Galactocentric radius r_{gc} , of the three velocity dispersion components σ_r , σ_θ , σ_ϕ , and anisotropy parameter β , for three metallicity bins, using our sample of halo K giants after efforts to remove Sagittarius stars as in Fig. 5. The top left, top right, and lower left panels show the three dispersion profiles, σ_r , σ_θ , σ_ϕ , respectively, divided into three metallicity bins. The lower right panel shows the anisotropy profile β . The two more metal rich bins share a common amplitude of $\beta \approx 0.9$ with $r_{gc} < 25$ kpc and gradually declining value of β at larger radii. The anisotropy profile is strikingly different for stars with $[\text{Fe}/\text{H}] < -1.8$, where the amplitude of β has dropped to ≈ 0.6 and remains relatively constant out to large radii; such stars are still on quite radial orbits, but substantially less so than the rest of the sample. This change in the underlying velocities used to form β can also be seen in the left-hand panels of Fig. 3. We note that substructure, particularly beyond ≈ 25 kpc, still is affecting β and the behavior should be regarded with care until careful structure identification and removal is performed.

we find for the halo K giants out to about 25 kpc. At a metallicity of $[\text{Fe}/\text{H}] \approx -2$, their Fig. 4 shows $\beta \approx 0.5$, quite similar to what we find ($\beta = 0.6$) in our most metal poor bin ($-2.5 < [\text{Fe}/\text{H}] < -1.8$). Beyond about 25 kpc, our sample becomes much more obviously affected by structure, and comparison with Belokurov et al. (2018) is not straightforward, but within 25 kpc the two samples do appear to be sampling a very

similar component of the Galactic halo in terms of the anisotropy dependence on $[\text{Fe}/\text{H}]$.

Fig. 8 shows a dip in β at a Galactocentric radius of approximately 15 kpc for the stars in the metallicity range $-1.8 < [\text{Fe}/\text{H}] < -1.5$. This is reminiscent of the dips seen in the halo simulations analyzed by Loebman et al. (2018), due to a disrupted satellite passage through a well-mixed background halo. Such dips would be short-lived and have metallicities restricted

to those of the dissolving satellite, as opposed to long-lived dips which involve stars in the in-situ halo, and thus no restriction to a particular range of metallicity. It will be interesting to see if this picture can be confirmed as part of an ongoing search for and analysis of streams amongst the LAMOST halo K giants.

4. CONCLUSIONS

The combination of distances and line-of-sight velocities from LAMOST, and proper motions from *Gaia*, demonstrate the power that 6-D surveys bring to Galactic structure and evolution studies. We have measured the anisotropy parameter β for K-giant stars in the Galactic halo, with metallicities $[\text{Fe}/\text{H}] < -1.3$, over a range of Galactocentric radii from 5 to over 100 kpc. We find that from the Solar position to about 25 kpc, the orbits are highly radial ($\beta \approx 0.8$) and then generally decline to near isothermality (with $\beta = 0.3$) to the limit of current measurements (~ 100 kpc). The anisotropy profile in the region $r_{\text{gc}} > 25$ kpc shows very clear signs of being affected by substructure, in line with expectations from N -body/hydrodynamical simulations of stellar halo formation and evolution around Milky Way-type galaxies (Loebman et al. 2018). Within the better relaxed region ($r_{\text{gc}} < 25$ kpc), our halo K giants share striking similarities with the halo main sequence star sample of Belokurov et al. (2018), who find very high anisotropy of $\beta \approx 0.9$ for the bulk of their stars, and a similar metallicity dependence, with orbits becoming more mildly radial with decreasing metallicity. We have compared our distance scale for nearby halo K giants (within 4 kpc) with that of Bailer-Jones et al. (2018) (based on *Gaia* parallaxes and priors for the stellar distribution in the Galaxy), finding that the scales differ by of order 10% (in the sense that our K giants have distances 10% closer than the estimates of Bailer-Jones et al. (2018)). The adoption of a Bailer-Jones et al. (2018) distance scale reduces the

anisotropy measure only slightly for our sample, leaving the overall conclusion of a highly radially anisotropic halo unchanged.

The end-of-mission *Gaia* proper motions will improve substantially over DR2, particularly for the more distant stars, so that we will be able to probe the anisotropy of the Galactic halo significantly better in the regions where it appears to be declining.

The determination of the total mass profile of the Milky Way (i.e. the enclosed mass as a function of Galactocentric radius) can be made using the Jeans equation and the full 6-D data for our sample: in the simplified case of a spherical Jeans equation, it is known that estimation of the mass profile is biased, even if β is known. The mass profile, although still subject to some sample bias, in particular due to non-virial effects, can be obtained using the 3-D version of the Jeans equation. The velocity dispersion profiles presented here will allow this, and we intend to measure the mass profile in a forthcoming paper.

We thank Warren Brown, Monica Valluri, Emily Cunningham, and Huang Yang for useful discussions. S.A.B. acknowledges support from the Postdoctoral Scholar’s Fellowship of LAMOST and the Chinese Academy of Sciences President’s International Fellowship Initiative Grant (no. 2016PE010) and the Aliyun Fellowship. The research presented here is partially supported by the 973 Program of China under grant no. 2014CB845700, by the National Natural Science Foundation of China under grant nos. 11773052, 11333003, 11761131016, and by a China-Chile joint grant from CASSACA. J.S. acknowledges support from a *Newton Advanced Fellowship* awarded by the Royal Society and the Newton Fund, and from the CAS/SAFEA International Partnership Program for Creative Research Teams. This work made use of the facilities of the Center for High Performance

Computing at Shanghai Astronomical Observatory. X.-X.X. acknowledges support from the “Recruitment Program of Global Youth Experts” of China and NSFC under grants 11390371, 11873052, and 11890694. C.F. acknowledges financial support by the Beckwith Trust. C.L. acknowledges the National Key Basic Research Program of China 2014CB845700 and the NSFC under grant 11333003. Guoshoujing Telescope (the Large Sky Area Multi-Object Fiber Spectroscopic Telescope LAMOST) is a National Major Scientific Project built by the Chinese Academy of Sciences. Funding for the project has been provided by the National Development and Reform Commission. LAMOST is operated and managed by the National Astronomical Observatories,

Chinese Academy of Sciences. This work has made use of data from the European Space Agency (ESA) mission *Gaia*, processed by the *Gaia* Data Processing and Analysis Consortium (DPAC). Funding for the DPAC has been provided by national institutions, in particular the institutions participating in the *Gaia* Multilateral Agreement. This research has made use of NASA’s Astrophysics Data System Bibliographic Services.

Software: **Astropy** (v2.0.2; [Astropy Collaboration et al. 2013, 2018](#)), **galpy** (1.3.0; [Bovy 2015](#)), **matplotlib.pyplot** (2.1.0; [Hunter 2007](#)), **NumPy** (v1.13.3; [Oliphant 2006; Walt et al. 2011; Oliphant 2015](#)), **ROBUST_SIGMA** ([Freudenreich et al. 1990-2009](#)); (**ASTROLIB**; [Landsman 1993](#)), **TOPCAT** (v4.3-3; [Taylor 2005](#))

REFERENCES

- Abadi, M. G., Navarro, J. F., & Steinmetz, M. 2006, *MNRAS*, 365, 747
- Ahn, C. P., Alexandroff, R., Allende Prieto, C., et al. 2012, *ApJS*, 203, 21
- An, D., Johnson, J. A., Clem, J. L., et al. 2008, *ApJS*, 179, 326
- Astropy Collaboration, Robitaille, T. P., Tollerud, E. J., et al. 2013, *A&A*, 558, A33
- Astropy Collaboration, Price-Whelan, A. M., Sipócz, B. M., et al. 2018, *AJ*, 156, 123
- Bailer-Jones, C. A. L., Rybizki, J., Foesneau, M., Mantelet, G., & Andrae, R. 2018, *AJ*, 156, 58
- Beers, T. C., Carollo, D., Ivezić, Ž., et al. 2012, *ApJ*, 746, 34
- Belokurov, V., Erkal, D., Evans, N. W., Koposov, S. E., & Deason, A. J. 2018, *MNRAS*, 478, 611
- Belokurov, V., Zucker, D. B., Evans, N. W., et al. 2006, *ApJ*, 642, L137
- Binney, J. 1980, *MNRAS*, 190, 873
- Binney, J., & Tremaine, S. 2008, *Galactic Dynamics: Second Edition* (Princeton University Press)
- Bovy, J. 2015, *ApJS*, 216, 29
- Bullock, J. S., & Johnston, K. V. 2005, *ApJ*, 635, 931
- Cambrésy, L., Jarrett, T. H., & Beichman, C. A. 2005, *A&A*, 435, 131
- Cardelli, J. A., Clayton, G. C., & Mathis, J. S. 1989, *ApJ*, 345, 245
- Carlin, J. L., Liu, C., Newberg, H. J., et al. 2016, *ApJ*, 822, 16
- Carollo, D., Beers, T. C., Lee, Y. S., et al. 2007, *Nature*, 450, 1020
- Chambers, K. C., Magnier, E. A., Metcalfe, N., et al. 2016, *ArXiv e-prints*, arXiv:1612.05560
- Chiba, M., & Yoshii, Y. 1998, *AJ*, 115, 168
- Christensen, C., Quinn, T., Governato, F., et al. 2012, *MNRAS*, 425, 3058
- Cui, X.-Q., Zhao, Y.-H., Chu, Y.-Q., et al. 2012, *Research in Astronomy and Astrophysics*, 12, 1197
- Cunningham, E. C., Deason, A. J., Guhathakurta, P., et al. 2016, *ApJ*, 820, 18
- Cutri, R. M., Skrutskie, M. F., van Dyk, S., et al. 2003, *VizieR Online Data Catalog*, 2246
- Deason, A. J., Belokurov, V., & Evans, N. W. 2011, *MNRAS*, 411, 1480
- Deason, A. J., Belokurov, V., Evans, N. W., & Johnston, K. V. 2013, *ApJ*, 763, 113
- Deng, L.-C., Newberg, H. J., Liu, C., et al. 2012, *Research in Astronomy and Astrophysics*, 12, 735
- Diemand, J., Madau, P., & Moore, B. 2005, *MNRAS*, 364, 367

- Fermani, F., & Schönrich, R. 2013, *MNRAS*, 432, 2402
- Freudenreich, H., Landsman, W., & Lim, P. L. 1990-2009, *ROBUST_SIGMA*
- Gaia Collaboration, Brown, A. G. A., Vallenari, A., et al. 2018, *A&A*, 616, A1
- Hakkila, J., Myers, J. M., Stidham, B. J., & Hartmann, D. H. 1997, *AJ*, 114, 2043
- Hattori, K., Valluri, M., Loebman, S. R., & Bell, E. F. 2017, *ApJ*, 841, 91
- Hattori, K., Yoshii, Y., Beers, T. C., Carollo, D., & Lee, Y. S. 2013, *ApJ*, 763, L17
- Henden, A., & Munari, U. 2014, *Contributions of the Astronomical Observatory Skalnaté Pleso*, 43, 518
- Henden, A. A., Levine, S., Terrell, D., & Welch, D. L. 2015, in *American Astronomical Society Meeting Abstracts*, Vol. 225, *American Astronomical Society Meeting Abstracts #225*, 336.16
- Henden, A. A., Templeton, M., Terrell, D., et al. 2016, *VizieR Online Data Catalog*, 2336
- Hunter, J. D. 2007, *Computing In Science & Engineering*, 9, 90
- Ibata, R. A., Gilmore, G., & Irwin, M. J. 1994, *Nature*, 370, 194
- Kafle, P. R., Sharma, S., Lewis, G. F., & Bland-Hawthorn, J. 2012, *ApJ*, 761, 98
- . 2013, *MNRAS*, 430, 2973
- . 2014, *ApJ*, 794, 59
- King, III, C., Brown, W. R., Geller, M. J., & Kenyon, S. J. 2015, *ApJ*, 813, 89
- Landsman, W. B. 1993, in *Astronomical Society of the Pacific Conference Series*, Vol. 52, *Astronomical Data Analysis Software and Systems II*, ed. R. J. Hanisch, R. J. V. Brissenden, & J. Barnes, 246
- Liu, C., Deng, L.-C., Carlin, J. L., et al. 2014, *ApJ*, 790, 110
- Loebman, S. R., Valluri, M., Hattori, K., et al. 2018, *ApJ*, 853, 196
- Luo, A.-L., Zhang, H.-T., Zhao, Y.-H., et al. 2012, *Research in Astronomy and Astrophysics*, 12, 1243
- Luo, A.-L., Zhao, Y.-H., Zhao, G., et al. 2015, *Research in Astronomy and Astrophysics*, 15, 1095
- Majewski, S. R., Skrutskie, M. F., Weinberg, M. D., & Ostheimer, J. C. 2003, *ApJ*, 599, 1082
- Morrison, H. L., Flynn, C., & Freeman, K. C. 1990, *AJ*, 100, 1191
- Oliphant, T. E. 2006, *A Guide to NumPy*, Vol. 1 (USA: Trelgol Publishing)
- . 2015, *Guide to NumPy: 2nd Edition* (USA: Continuum Press)
- Rashkov, V., Pillepich, A., Deason, A. J., et al. 2013, *ApJ*, 773, L32
- Robin, A. C., Bienaymé, O., Fernández-Trincado, J. G., & Reylé, C. 2017, *A&A*, 605, A1
- Schlafly, E. F., & Finkbeiner, D. P. 2011, *ApJ*, 737, 103
- Schlafly, E. F., Finkbeiner, D. P., Jurić, M., et al. 2012, *ApJ*, 756, 158
- Schlegel, D. J., Finkbeiner, D. P., & Davis, M. 1998, *ApJ*, 500, 525
- Schönrich, R., Asplund, M., & Casagrande, L. 2011, *MNRAS*, 415, 3807
- Schönrich, R., & Aumer, M. 2017, *MNRAS*, 472, 3979
- Schönrich, R., Binney, J., & Dehnen, W. 2010, *MNRAS*, 403, 1829
- Skrutskie, M. F., Cutri, R. M., Stiening, R., et al. 2006, *AJ*, 131, 1163
- Smith, M. C., Evans, N. W., Belokurov, V., et al. 2009, *MNRAS*, 399, 1223
- Sommer-Larsen, J., Flynn, C., & Christensen, P. R. 1994, *MNRAS*, 271, 94
- Stinson, G. S., Brook, C., Macciò, A. V., et al. 2013, *MNRAS*, 428, 129
- Taylor, M. B. 2005, in *Astronomical Society of the Pacific Conference Series*, Vol. 347, *Astronomical Data Analysis Software and Systems XIV*, ed. P. Shopbell, M. Britton, & R. Ebert, 29
- Thom, C., Flynn, C., Bessell, M. S., et al. 2005, *MNRAS*, 360, 354
- Tian, H.-J., Liu, C., Carlin, J. L., et al. 2015, *ApJ*, 809, 145
- Walt, S. v. d., Colbert, S. C., & Varoquaux, G. 2011, *Computing in Science & Engineering*, 13, 22
- Wu, Y., Du, B., Luo, A., Zhao, Y., & Yuan, H. 2014, in *IAU Symposium*, Vol. 306, *Statistical Challenges in 21st Century Cosmology*, ed. A. Heavens, J.-L. Starck, & A. Krone-Martins, 340–342
- Wu, Y., Luo, A.-L., Li, H.-N., et al. 2011, *Research in Astronomy and Astrophysics*, 11, 924

Xue, X.-X., Ma, Z., Rix, H.-W., et al. 2014, ApJ,
784, 170

Yanny, B., Rockosi, C., Newberg, H. J., et al.
2009, AJ, 137, 4377
Zhao, G., Zhao, Y.-H., Chu, Y.-Q., Jing, Y.-P., &
Deng, L.-C. 2012, RAA, 12, 723